



OPEN

Induction of mitochondria-mediated apoptosis and suppression of tumor growth in zebrafish xenograft model by cyclic dipeptides identified from *Exiguobacterium acetylicum*

Sekar Jinendiran¹, Weilin Teng², Hans-Uwe Dahms^{3,4}✉, Wangta Liu²,
Vinoth Kumar Ponnusamy⁵, Charles Chien-Chih Chiu², B. S. Dileep Kumar⁶✉ &
Natesan Sivakumar¹✉

Colorectal cancer is the most common type of gastrointestinal cancers with poor survival and limited therapeutic options. In this study, four structurally different cyclic dipeptides (or diketopiperazine) were isolated and identified as cyclo (L-Pro-L-Leu), cyclo (L-Pro-L-Val), cyclo (L-Pro-L-Phe) and cyclo (L-Pro-L-Tyr) from the ethyl acetate extract in the cell-free filtrate of *Exiguobacterium acetylicum* S01. The anticancer potential of identified DKPs on colorectal cancer HT-29 cells in vitro and in vivo zebrafish xenograft model was evaluated. The MTT (3-(4, 5-dimethylthiazol-2yl)-2, 5-diphenyltetrazolium bromide) assay showed that four DKPs exhibited significant inhibition of HT-29 cells viability in a dose-dependent manner whereas there were no cytotoxic effects on normal mouse fibroblast 3T3 cells. Also, we observed that all DKPs induce early and late apoptotic cell death in HT-29 cells. Moreover, the expression levels of apoptotic (cytochrome-c, caspase-3 and Bid) and anti-apoptotic (Bcl-2) markers were up- and down-regulated in HT-29 cells in response to DKPs treatments. Furthermore, these four DKPs remarkably inhibited the tumor progression in a zebrafish xenograft model within a nonlethal dose range. Overall, our findings suggest that cyclic dipeptides derived from *E. acetylicum* S01 could be promising chemopreventive/therapeutic candidates against cancer.

Colorectal cancer (CRC) is the third most commonly diagnosed malignancy and the second leading cause of cancer-related deaths in the world. According to the World Health Organization reports, the global burden of CRC is expected to increase by 60% i.e., 2.2 million new cases and 1.1 million deaths by the year 2030¹. The risk factor for developing CRC is connected with age, genetic predisposition, disease history, and lifestyle including

¹Department of Molecular Microbiology, School of Biotechnology, Madurai Kamaraj University, Madurai 625021, India. ²Department of Biotechnology, Kaohsiung Medical University, Kaohsiung 80708, Taiwan. ³Department of Biomedical Science and Environmental Biology, Kaohsiung Medical University, Kaohsiung 80708, Taiwan. ⁴Department of Marine Biotechnology and Bioresources, National Sun Yat-Sen University, Kaohsiung 80424, Taiwan. ⁵Department of Medicinal Applied Chemistry, Kaohsiung Medical University, Kaohsiung 80708, Taiwan. ⁶Agro-Processing and Technology Division, CSIR-National Institute for Interdisciplinary Science and Technology, Thiruvananthapuram 695019, India. ✉email: hansd@kmu.edu.tw; kumardileep@niist.res.in; sivamku.ac@gmail.com

food habits. Also, the development of tumor proceeds through a series of genetic and epigenetic alterations involving the activation of oncogenes and inactivation of tumor suppressor genes^{1,2}. The progressive inhibition of apoptosis in CRC has been found during the cellular transformation of the normal intestinal epithelium to adenocarcinomas³, which contribute to promoting neoplastic progression and resistance to anticancer drugs⁴. However, 5-fluorouracil (5-FU)-based chemotherapy is the most common treatments for the early stage of CRC⁴. At the metastatic stage, the cancer is generally unresponsive to available therapies and thus is commonly fatal². Therefore, there is a need to develop a novel therapeutic approach that is more effective than currently used treatment regimens. In this perspective, the use of cyclic peptides is receiving considerable attention as an alternative therapeutic agent against CRC^{5,6}.

Cyclic dipeptides (or diketopiperazine—DKP) are organic substances formed by two amino acids joined by covalent bonds known as amide or peptide bonds. These dipeptides are an important class of biologically active molecules. They are produced by a wide range of organism encompassing both Gram-positive and Gram-negative bacteria, fungi, sponges, and animals⁷. Several cyclic dipeptides have diverse biological functions, such as anti-microbial, antifungal, antiviral, anti-inflammatory, anticancer, and immunosuppressive activities^{8,9}. Nishanth Kumar and co-workers reported that cyclo (D-Tyr-D-Phe) isolated from *Bacillus* sp, which induces apoptosis by the activation of caspase-3 in a pulmonary adenocarcinoma cell line¹⁰. Another report established that cyclo (L-Phe-L-His) obtained from *Aspergillus ustus* and cyclo (L-Phe-L-Pro) isolated from the probiotic strain *Lactobacillus plantarum* inhibits the growth of various cancer cells^{11,12}. Moreover, earlier studies demonstrated that a crude mixture of DKPs obtained from the *Pseudomonas aeruginosa* PAO1 strain, which promotes apoptotic cell death in HeLa and Caco-2 cells¹³.

In recent years, several studies showed that deregulated proliferation and inhibition of the apoptotic process is a critical factor for all tumor development. Therefore, the regulation of cell growth and apoptosis affords an evident target for therapeutic intervention in all cancers¹⁴. In general, apoptosis can be induced either by an extrinsic pathway mediated through the activation of death receptors or by an intrinsic signalling pathway, which involves in the alteration of mitochondrial membrane permeability (MMP), thereby inducing the release of cytochrome-c from mitochondria^{15,16}. This intrinsic pathway is regulated by the Bcl-2 family of proteins, which controls MMP¹⁷. Recently, zebrafish is an emerging animal model for examining tumors¹⁸ and tumor–organ interaction due to many advantages. Thus, zebrafish xenograft model is receiving considerable attention as a reliable whole-animal model system to rapidly screen for small-molecule as drug candidates^{19,20}. However, the purification and characterization of DKPs from the potentially probiotic strain *Exiguobacterium acetylicum* S01 and their therapeutic efficacy on CRC have not yet been studied extensively. Hence, the objective of the present investigation was aimed to isolate and identify DKPs from the cell-free extract of *E. acetylicum* S01 and to evaluate their therapeutic potential in colorectal cancer HT-29 cells in vitro and in vivo zebrafish xenograft model.

Results

Purification of bioactive metabolites. The oily reddish-yellow extract was obtained from the cell-free culture filtrate of *E. acetylicum* S01. The crude extract was taken for purification of bioactive metabolites using silica gel column chromatography (SGCC) following the method described by Nishanth Kumar et al.²¹ with slight modification. Column chromatography of this extract yielded four crystalline compounds eluted at 45% ethyl acetate in hexane (DKP-1), 55% ethyl acetate in hexane (DKP-2), 70% ethyl acetate in hexane (DKP-3), and 5% methanol in chloroform (DKP-4) respectively. Thin-layer chromatography of the eluted all DKPs in silica gel TLC sheets demonstrated single spots.

Structural elucidation of bioactive compounds. Structures of purified compounds were elucidated by ¹H and ¹³C NMR and mass spectrometric analysis (HR-ESI-MS). The compounds isolated from *E. acetylicum* S01 were identified as cyclo (L-Pro-L-Leu) (DKP-1), cyclo (L-Pro-L-Val) (DKP-2), cyclo (L-Pro-L-Phe) (DKP-3), and cyclo (L-Pro-L-Tyr) (DKP-4) (Fig. 1). Both ¹H and ¹³C NMR spectra of all DKPs exhibited a signal at δH 4.13 (t) with *J* value around 8 Hz with a corresponding δC of 59.0, together with multiplets around δH 2.3, 2.0, and 3.5 ppm, which shows the presence of a proline residue. The amide hydrogen signal in ¹H NMR spectra of all DKPs, and comparison with standard amino acids, and all DKPs presently identified were found to have proline. The absolute configuration was determined by digital polarimeter and by comparison against reported specific rotation values of the respective compound^{22–24}.

DKP 1: Cyclo (L-Pro-L-Leu). Yellow crystalline powder 55 mg; TLC (hexane: ethyl acetate, 80:20 v/v): R_f=0.50; HPLC (methanol (MeOH): acetonitrile (CH₃CN), 70:30 v/v): RT=0.96 min; Specific Optical Rotation: [α]²⁴_D 124° (*c*=0.3, ethanol), for R,R [α]²⁴_D = −124° (*c*=0.4, ethanol)²²; ¹H and ¹³C NMR data, see Table 1 (Fig. S1A, B); HR-ESI-MS (*m/z*): [M + H]⁺ calcd for C₁₁H₁₉N₂O₂, 211.1450; found, 211.1446 (Fig. S2A).

DKP 2: Cyclo (L-Pro-L-Val). Pale yellow crystalline powder 41 mg; TLC (hexane: ethyl acetate, 20:80 v/v): R_f=0.6; HPLC (MeOH:CH₃CN, 70:30 v/v): RT=0.97 min; Specific Optical Rotation: [α]²⁴_D = −144° (*c*=0.3, ethanol), for R,R, [α]²⁰_D = −139.4° (*c*=0.16, EtOH)²³; ¹H and ¹³C NMR data, see Table 1 (Fig. S1C,D); HR-ESI-MS (*m/z*): [M + H]⁺ calcd for C₁₀H₁₇N₂O₂, 197.1292; found, 197.1290 (Fig. S2B).

DKP 3: Cyclo (L-Pro-L-Phe). Pale yellow powder (9.5 mg); TLC (hexane: ethyl acetate, 10:90 v/v): R_f=0.3; HPLC (MeOH:CH₃CN, 60:40 v/v): RT value 0.86 min; Specific Optical Rotation: [α]²⁴_D = −82° (*c*=0.4, MeOH), for R,R, [α]²⁵_D = −92° (*c*=1.1, MeOH)²⁴; ¹H and ¹³C NMR data, see Table 1 (Fig. S1E,F); HR-ESI-MS (*m/z*): [M + H]⁺ calcd for C₁₄H₁₇N₂O₃, 245.1292; found, 245.1290 (Fig. S2C).

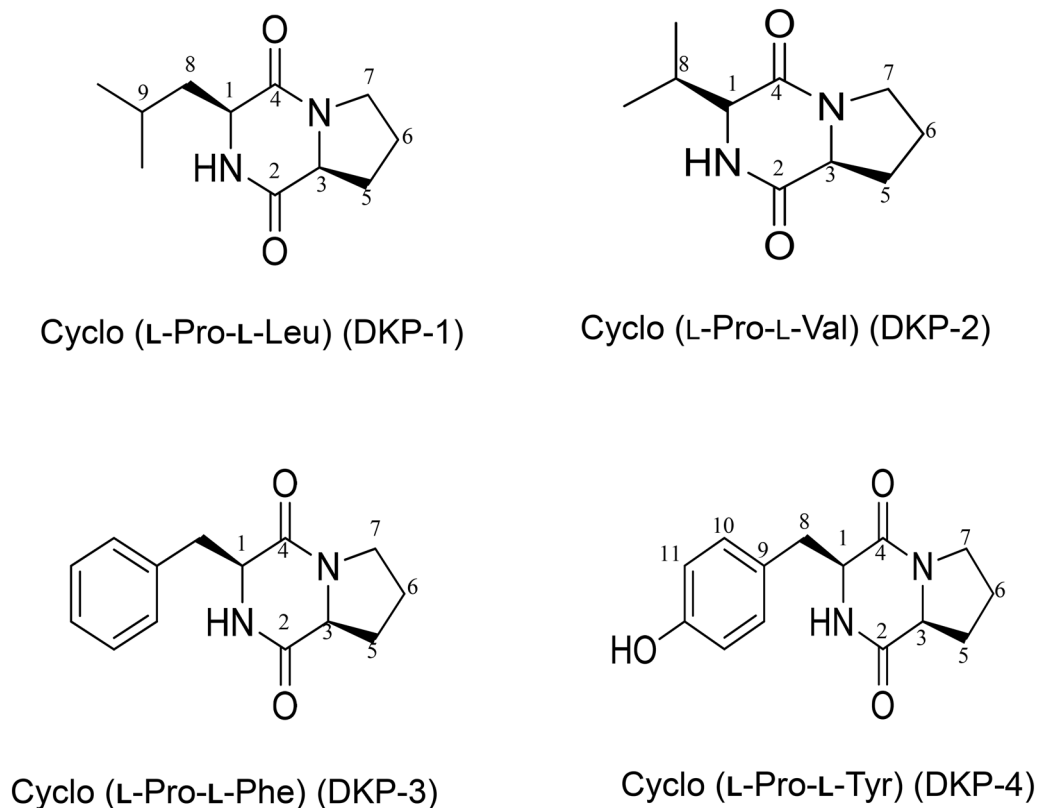


Figure 1. Structures of isolated cyclic dipeptides from the ethyl acetate extract in the cell-free filtrate of *E. acetylicum* S01. Chemical structures of the four cyclic dipeptides identified from *E. acetylicum* S01.

Carbon No	DKP-1		DKP-2		DKP-3		DKP-4	
	δ H	δ C	δ H	δ C	δ H	δ C	δ H	δ C
1	4.02, dd (7)	53.4	3.87 (s)	60.4	4.20, dd (10.5, 3)	56.1	4.20, dd (3.5, 11.5)	56.2
OH							4.15, dd (9.5, 2.5)	
NH	6.21 (s)		6.19 (s)		5.57 (s)		5.93 (s)	
2		166.2		164.9		165.0		165.2
3	4.13, t (8.0)	58.9	4.01, app t, (8)	58.8	4.01, t (7.5)	59.1	4.0, td (5.5, 7.5)	59.1
4		170.2		170.1		169.3		169.7
5	2.33, 2.37, m	28.1	2.28, 2.33, m	28.4	1.93, 1.96, 2.24, 2.29, m	28.3	1.96, 2.27, m	28.3
6	2.02, 2.18, m	24.6	1.93, 2.02, m	22.3	1.18, 1.85, m	22.5	1.89, m	22.4
7	3.52, 3.64, m	45.5	3.49, 3.60, m	45.1	3.59, m	45.4	3.50, 3.59, m	45.4
8	1.17, 1.82, 1.88, 1.94, m	38.6	1.17, 1.88, 1.93, 2.02, m	28.5	2.71, dd (14.5, 10.5)	36.8	2.71, dd (14.5, 9.5), 3.37, dd (14.5, 4)	35.9
9	1.54, ddd (14.5, 9.5, 5)	23.2	2.54, ddd (2.5)	19.1				126.8
10	1.01, d (6.5)	22.7	1.01, d (7)	19.0			6.97, d (8.5 H10,10')	130.3
11	0.96, d (6.5)	21.2	0.84, d (7)				6.70, d (8.5 H11,11')	116.1
12								155.7
Ph					7.15–7.30	127.5, 129.1, 129.2, 135.9		

Table 1. NMR data for DKPs 1 – 4 in CDCl_3 (multi, J , Hz). *s* singlet; *d* doublet; *dd* doublet of doublets; *m* multiplet; *t* triplet.

DKP 4: Cyclo (L-Pro-L-Tyr). Pale yellow powder (25.5 mg); TLC (methanol: chloroform, 1:99 v/v): $R_f = 0.80$; HPLC (MeOH: CH_3CN , 50:50 v/v): $RT = 0.99$ min; Specific Optical Rotation: $[\alpha]_D^{25} = -106^\circ$ ($c = 0.5$, MeOH), for R,R, $[\alpha]_D^{25} = -100^\circ$ ($c = 0.5$, MeOH)²⁴; ^1H and ^{13}C NMR data, see Table 1 (Fig. S1G,H); HR-ESI-MS (m/z): $[M + \text{H}]^+$ calcd for $\text{C}_{14}\text{H}_{17}\text{N}_2\text{O}_3$, 261.1241; found, 261.1239 (Fig. S2D).

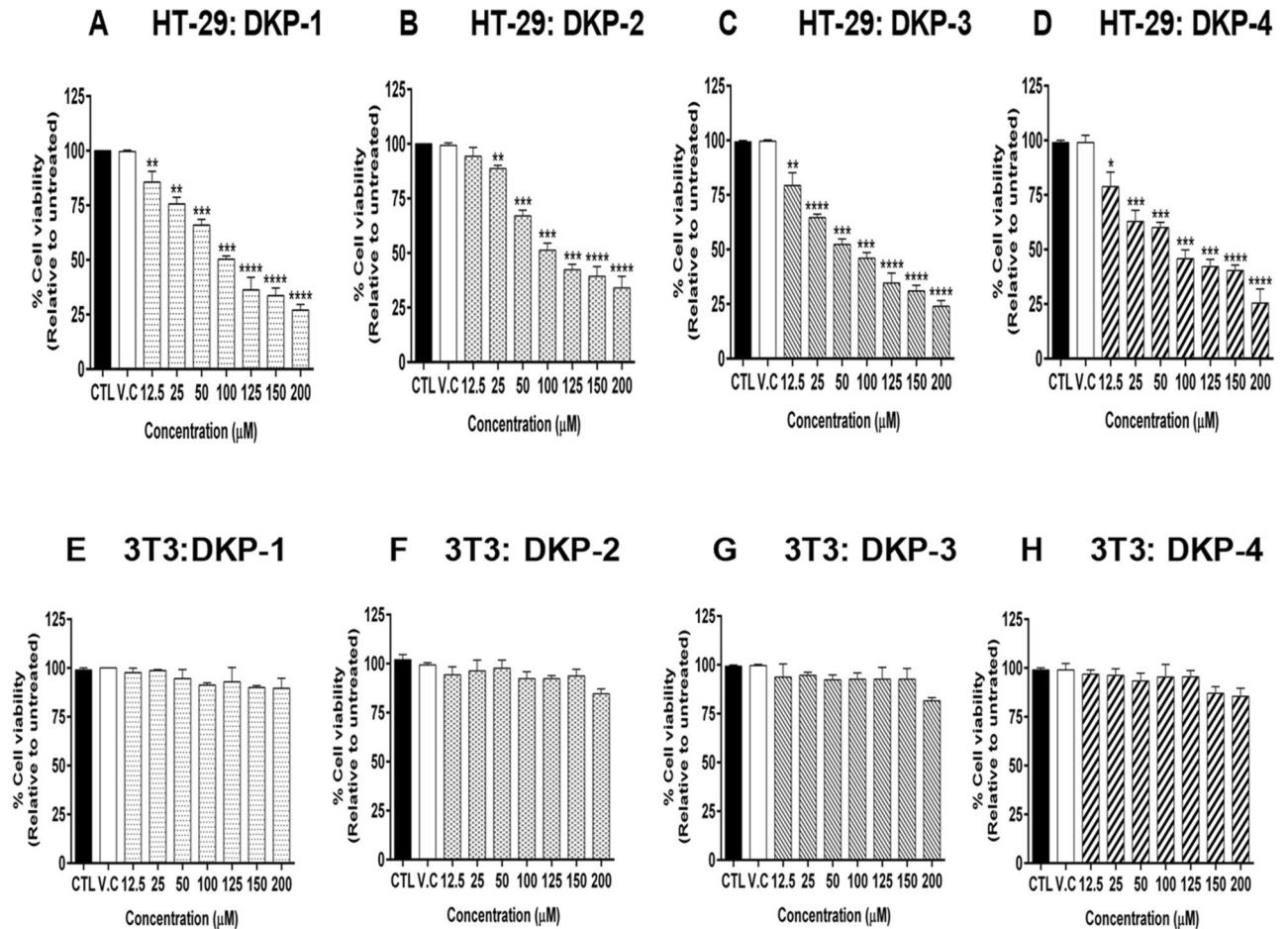


Figure 2. Cell viability in cells treated with cyclic dipeptides (DKPs). (A–D) Colorectal cancer HT-29 cells were treated with different doses of DKP-1: cyclo (L-Pro-L-Leu) (A), DKP-2: cyclo (L-Pro-L-Val) (B), DKP-3: cyclo (L-Pro-L-Phe) (C), and DKP-4: cyclo (L-Pro-L-Tyr) (D) for 24 h. (E–H) Normal mouse fibroblast 3T3 cells were treated with different doses of DKP-1 (E), DKP-2 (F), DKP-3 (G), and DKP-4 (H) for 24 h. Cell viability was determined relative to the untreated cells or vehicle control. Data were expressed as mean \pm SD ($n=3$). Data were analyzed by one-way ANOVA with student's two-tailed t -test. The asterisks * $p < 0.05$, ** $p < 0.001$, *** $p < 0.0001$, **** $p < 0.0001$, indicates a significant difference between the control in response to DKPs treatments. CTL Control; VC Vehicle control (DMSO).

Effects of DKPs on cell viability of cancer and normal cells. MTT assay revealed that the four DKPs affected the viability of HT-29 cells in a dose-dependent manner when compared with untreated or DMSO treated cells (Fig. 2). After 24 h treatment with a 125 μM dose of four DKPs, the relative percentage viability of HT-29 cells was $36.33 \pm 5.08\%$ (DKP-1), $42.33 \pm 2.25\%$ (DKP-2), $34.66 \pm 4.03\%$ (DKP-3), and $42.15 \pm 2.94\%$ (DKP-4) (Fig. 2A–D). Colorectal cancer HT-29 cells inhibitory (IC_{50}) doses were for 100.5 μM (DKP-1), 117.70 μM (DKP-2), 85.19 μM (DKP-3), and 97.97 μM (DKP-4). Mouse embryonic fibroblast (3T3) cells were used as control cells to compare the cytotoxic effects of DKPs in tumor and normal cells. The results showed that all DKPs did not exhibit a significant cytotoxic effect in 3T3 cells, while we observed the viability loss of $> 10\%$ in the higher dose of 200 μM treated cells (Fig. 2E–H). Moreover, these four DKPs were exhibited promising antiproliferative activity against HT-29 cells in this study.

Induction of apoptosis by DKPs in HT-29 cells. To determine whether the growth inhibitory effects of DKPs were linked to the induction of apoptosis by annexin V-FITC and propidium iodide staining was evaluated. We found that treatment of HT-29 cells with DKPs for 24 h increased the number of early (PI $^-$ /AV $^+$; Q3) and late apoptotic or necrotic (PI $^+$ /AV $^+$; Q2) cells in a dose-dependent manner (Fig. 3 and Table 2). Also, we observed that the populations of dead cells (PI $^+$ /AV $^-$; Q1) have changed, 3.1-fold (DKP-1), 3.0-fold (DKP-2), 1.7-fold (DKP-3), and 2.1-fold (DKP-4) at a dose of 100 μM DKP-1–2, 50 μM DKP-3, and 200 μM DKP-4 treated cells when compared with untreated cells (Fig. 3 and Table 2). Moreover, both dead (Q1 + Q2) and apoptotic (Q2 + Q3) cell populations were significantly higher in the DKPs treatments compared to the control (Table 2). However, apoptotic cells were differentiated from necrotic cells by co-staining with PI because PI stains necrotic cells and it was excluded from live and early apoptotic cells due to the presence of an intact plasma membrane. This result revealed that DKPs inhibits the growth of HT-29 cells by the induction of apoptosis.

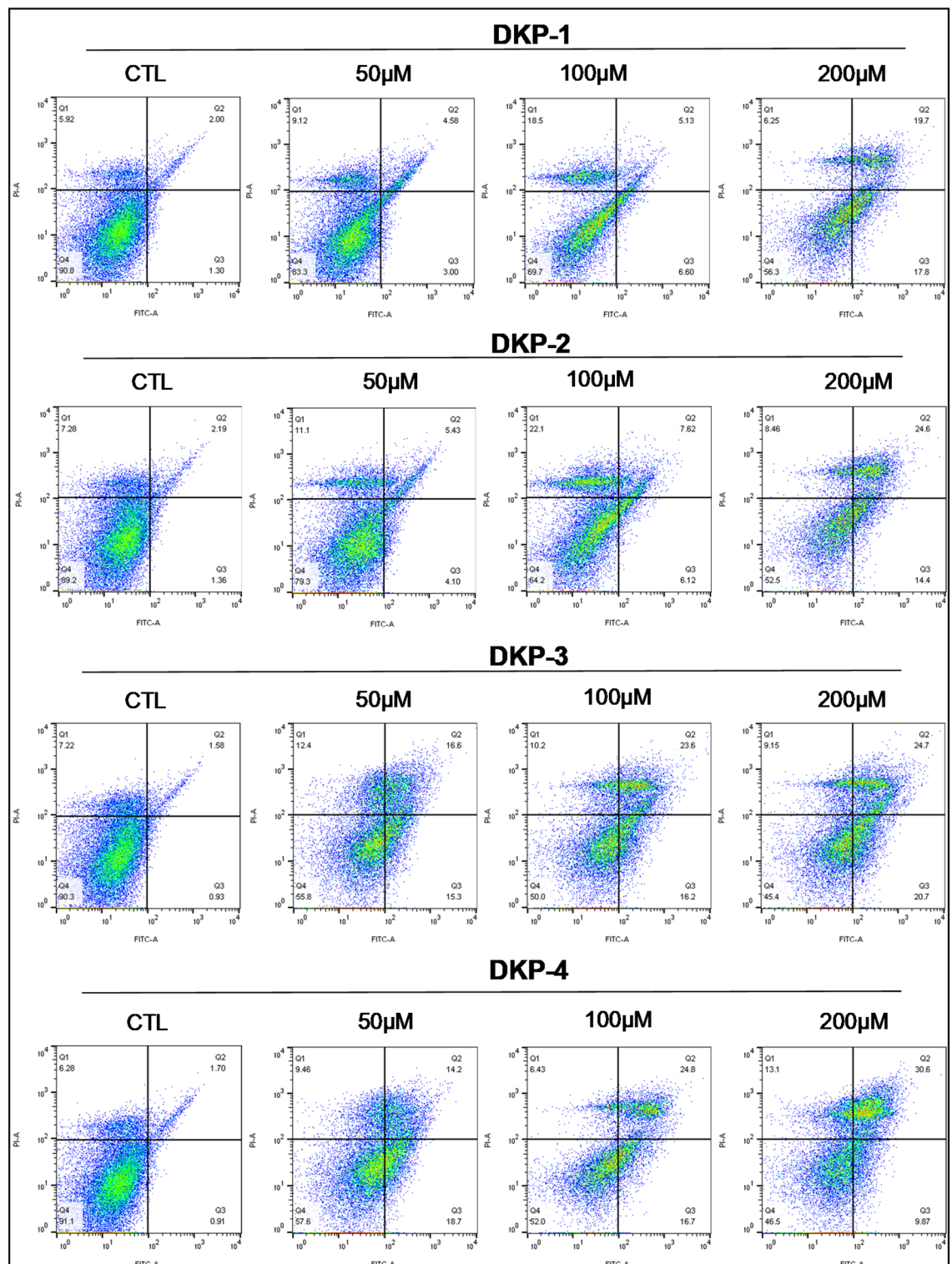


Figure 3. Cyclic dipeptide induces apoptosis in HT-29 cells. Annexin V-FITC/PI double staining was performed to analyze apoptotic cell populations by flow cytometry. HT-29 cells were treated with different doses (50, 100 and 200 μ M) of four DKPs as indicated for 24 h. Percentage of the dead (Q1), late apoptotic/necrotic (Q2), early apoptotic (Q3) and viable (Q4) cells were shown in quadrant plot. CTL Control.

Effects of DKPs on the expression of apoptosis-related genes. The expression levels of Cytc and Casp-3 were significantly ($p < 0.001$) up-regulated in a dose-dependent manner in response to DKPs treatments compared to the control (untreated cells) (Fig. 4). Cytc levels were significantly up-regulated, 2.32-fold, 1.78-

Concentration in μM	Q1	EAC Q3	LA/NC Q2	Q1 + Q2	Q2 + Q3
Fold changes					
DKP-1: HT-29					
CTL	1.0	1.0	1.0	1.0	1.0
50	1.5	0.4	2.3	1.7	2.3
100	3.1	0.9	2.6	3.0	3.6
200	1.1	2.4	9.9	3.3	11.4
DKP-2: HT-29					
CTL	1.0	1.0	1.0	1.0	1.0
50	1.5	3.0	2.5	1.7	2.7
100	3.0	4.5	3.5	3.1	3.9
200	1.2	10.6	11.2	3.5	11.0
DKP-3: HT-29					
CTL	1.0	1.0	1.0	1.0	1.0
50	1.7	16.5	10.5	3.3	12.7
100	1.4	17.4	14.9	3.8	15.9
200	1.3	22.3	15.6	3.8	18.1
DKP-4: HT-29					
CTL	1.0	1.0	1.0	1.0	1.0
50	1.5	20.5	8.4	3.0	12.6
100	1.0	18.4	14.6	3.9	15.9
200	2.1	10.8	18.0	5.5	15.5

Table 2. Cyclic dipeptides induces apoptosis in HT-29 cells in a dose-dependent manner. Annexin V-FITC/PI double staining was performed to analyze apoptotic cell populations. HT-29 cells were treated with different doses of four DKPs as an indicated time for 24 h. Data are representative of three independent experiments ($n=3$). DKP -1—cyclo (L-Pro-L-Leu), DKP -2—cyclo (L-Pro-L-Val), DKP -3—cyclo (L-Pro-L-Phe), and DKP -4—cyclo (L-Pro-L-Tyr). CTL Control, Dead cells (Q1), EAC—early apoptotic cells (Q3), LA/NC—late apoptotic or/and necrotic cells (Q2), Q1 + Q2— total dead cells, Q2 + Q3—total apoptotic cells.

fold, 4.29-fold, and 3.62-fold, respectively, in DKP-1, DKP-2, DKP-3 and DKP-4 at a dose of 200 μM compared with untreated cells ($p=0.001$; Fig. 4A–D). Similarly, Casp-3 gene expression was up-regulated, 2.32-fold (DKP-1), 1.31-fold (DKP-2), 1.76-fold (DKP-3), and 2.73-fold (DKP-4) at a dose of 200 μM DKPs treated cells compared with untreated cells ($p=0.0001$; Fig. 4A–D). Interestingly, the anti-apoptotic gene (Bcl-2) expression level was significantly down-regulated in HT-29 cells in response to DKPs treatments compared to the control. Moreover, the induction of apoptosis by DKPs was linked with the suppressed mRNA expression level of Bcl-2 in HT-29 cells (Fig. 4A–D).

Effect of DKPs on the expression of apoptotic proteins. The expression of apoptosis-related proteins (Cytc and Bid) following DKPs treatment were evaluated by Western blot analysis to further determine the mechanism of DKPs induced apoptosis. We observed that all DKPs had a significant increase in the expression levels of apoptotic proteins compared with untreated cells (Fig. 5). Cytc expression was significantly up-regulated, 1.21-fold (DKP-1), 1.45-fold (DKP-3), and 1.85-fold (DKP-4), at a dose of 100 μM of DKPs treatment compared with untreated cells ($p=0.0040$, $p=0.0045$, and $p=0.0001$, respectively; Fig. 6A–D). In contrast, the expression levels were slightly decreased at a dose of 200 μM treated cells compared to lower doses of 50 μM and 100 μM respectively (Fig. 5A,C,D). Likewise, the Bid expression was up-regulated, 1.32-fold 1.21-fold 1.76-fold, respectively in DKP-1, DKP-2 and DKP-3 at a treatment dose of 200 μM compared to the untreated group ($P<0.001$) (Fig. 5A–D). Interestingly, we found that DKP-4 treatment with a lower dose of 100 μM increased the expression level of Bid when compared with control and the higher dose of 200 μM treated HT-29 cells (Fig. 5C). Further, the expression level of Cytc was increased in the cytosolic fraction in response to DKPs treatments, whereas the level of Cytc decreased in the mitochondrial fraction (Fig. 5E,H) when compared to the untreated cells. Moreover, this result indicated that Cytc was released from mitochondria into the cytosol in a concentration-dependent manner and also triggered the mitochondria-mediated apoptotic cascade.

Effects of DKPs on zebrafish embryo developmental toxicity. Zebrafish (ABiC) embryos were treated with different doses of four DKPs for 96 hpf. At every 24 h time interval, the survival rate and developmental changes of the embryos were observed by inverted fluorescence microscope. We observed no significant decrease in the survival rate of embryos treated with various doses (50, 100 and 150 μM) of three DKPs (DKP-1, DKP-2 and DKP-4) treatments compared with untreated embryos as well as DMSO treated embryos at 96 hpf. Also, the survival rates of embryos were slightly higher in the treatment groups compared to the control (Table 3). The survival rate was higher at lower doses (50 and 150 μM) of DKP-3 treated embryos, whereas the survival rate was slightly reduced at the higher dose of 200 μM treated embryos compared with untreated

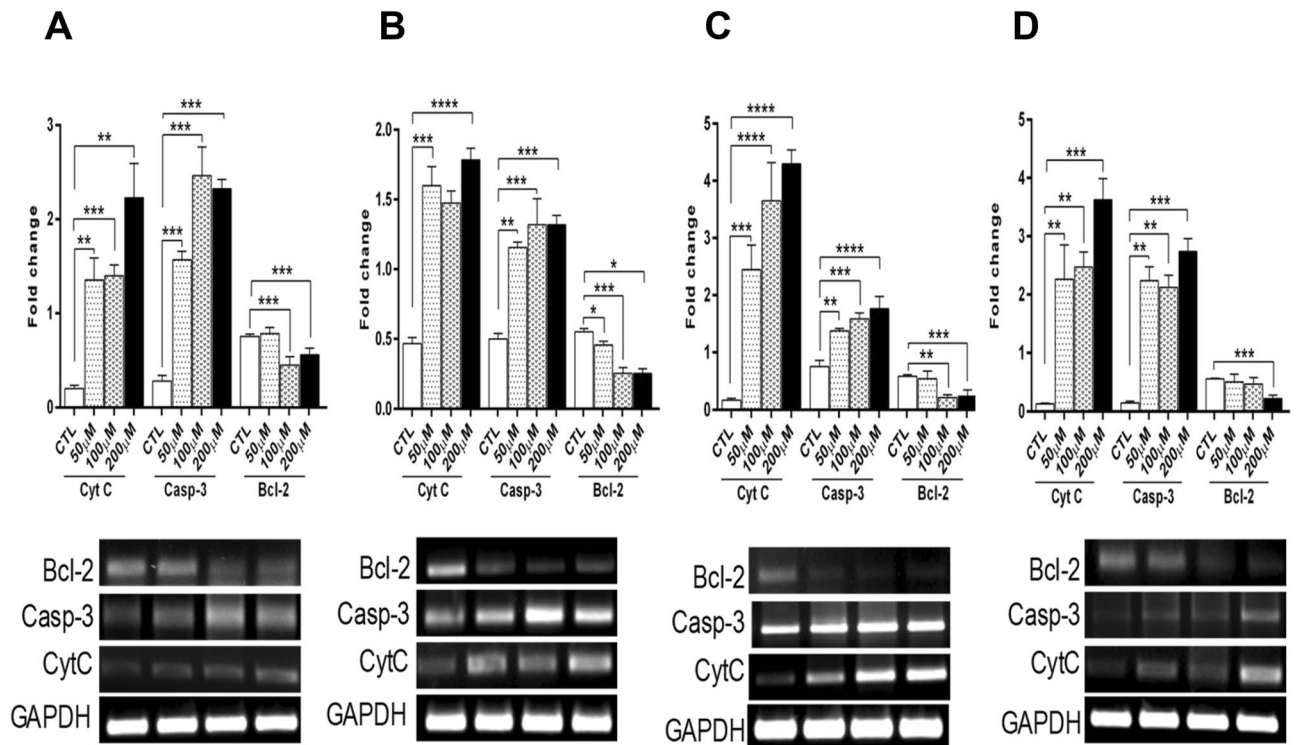


Figure 4. Apoptotic and anti-apoptotic gene expression levels in DKPs treated and un-treated HT-29 cells for 24 h. DKP-1: cyclo (L-Pro-L-Leu) (A), DKP-2: cyclo (L-Pro-L-Val) (B), DKP-3: cyclo (L-Pro-L-Phe) (C), and DKP-4: cyclo (L-Pro-L-Tyr) (D). The sqRT-PCR analysis was performed in triplicates, and each bar represents the mean \pm SD ($n = 3$). Data were analyzed by one-way ANOVA with student's two-tailed t -test. The asterisks $*p < 0.05$, $**p < 0.001$, $***p < 0.0001$, $****p < 0.0001$, indicates a significant difference between the untreated cells in response to DKPs treated cells. The groupings were cropped from different gels subjected to identical conditions. Full gel images were shown in the Supplementary Information, Fig. S3A–D.

embryos (Table 3). Moreover, we confirmed the morphological features of the zebrafish embryos after treatment with four DKPs using an inverted microscope. As evident from the images, all the DKPs did not show any adverse effects on the developmental toxicity or teratogenic effect on the embryos at 24, 48, and 72 hpf exposure (Fig. 6). Furthermore, beyond 96 hpf exposures at a higher dose of 200 μ M, all DKPs, none of the DKPs showed any side effects on the embryonic development of the zebrafish (Fig. 6A–D).

Anti-cancer effects of dipeptides in a xenograft model. The antitumor effects of all DKPs were further investigated in a zebrafish xenograft model. We observed a significant ($p < 0.001$) reduction in the fluorescence intensity and inhibition of tumor growth ($> 30\%$) by DKP-2, DKP-3, and DKP-4 compared with control and treatment with DKP-1, after 24 hpi (Fig. 7 and Fig. S5). After 48 hpi, the inhibition of tumor growth rate was significantly increased, 57% (DKP-1), 58% (DKP-2), 68% (DKP-3), and 60% (DKP-4), in the dose of 200 μ M treated cells compared to the untreated cells ($p = 0.0001$, $p = 0.0049$, $p = 0.0174$, and $p = 0.0123$, respectively; Figs. 7 and S5). Moreover, tumor growth was significantly reduced at the dose of 200 μ M treated embryos; DKP-1 (68%), DKP-2 (78%), DKP-3 (81%) and DKP-4 (74%) compared with control embryos at 72 hpi. At all time intervals, zebrafish were treated with different doses of DKP-3 exhibited the highest tumor growth inhibition rates when compared to other peptides used in this study (Figs. 7; S5). Furthermore, the survival rate was slightly reduced in response to DKPs treatment compared to the control, after 48 hpi and 72 hpi (Figs. 7; S5).

Discussion

Several investigations demonstrated the reduced risk of developing CRC in humans consuming diets rich in probiotics²⁶. The principle probiotics derived agents such as cyclic peptides, conjugated linoleic acids (CLAs) and short-chain fatty acids (SCFAs) could protect against cancer and infectious diseases^{26,27}. Among them, DKPs were demonstrated to exert their effects on various biological functions including inhibiting the cell cycle, inducing apoptosis, reducing oxidative stress, and stimulating the immune responses^{5,26}. In this study, the viability assay revealed that four DKPs induced growth arrest in HT-29 cells in a dose-dependent manner. Subtle structural variances are known to play a vital role in the inhibition of all DKPs. Besides, the tested four DKPs did not exhibit a cytotoxic effect on normal 3T3 cells compared to the untreated cells. The growth-inhibitory effects of DKPs are similar to the previous report on similar groups of compounds, where cyclo (Phe-Pro) and cyclo (Tyr-Pro) exhibited 50% growth inhibition of HT-29, HeLa, and MCF-7 cells in a dose-dependent manner after treatment with a dose of fewer than 7 mM¹². The crude mixture of DKPs obtained from *P. aeruginosa* PAO1 strain, mainly comprised of cyclo (L-Pro-L-Val), cyclo (L-Pro-L-Try), and cyclo (L-Pro-L-Phe), induced cell death in cervical and

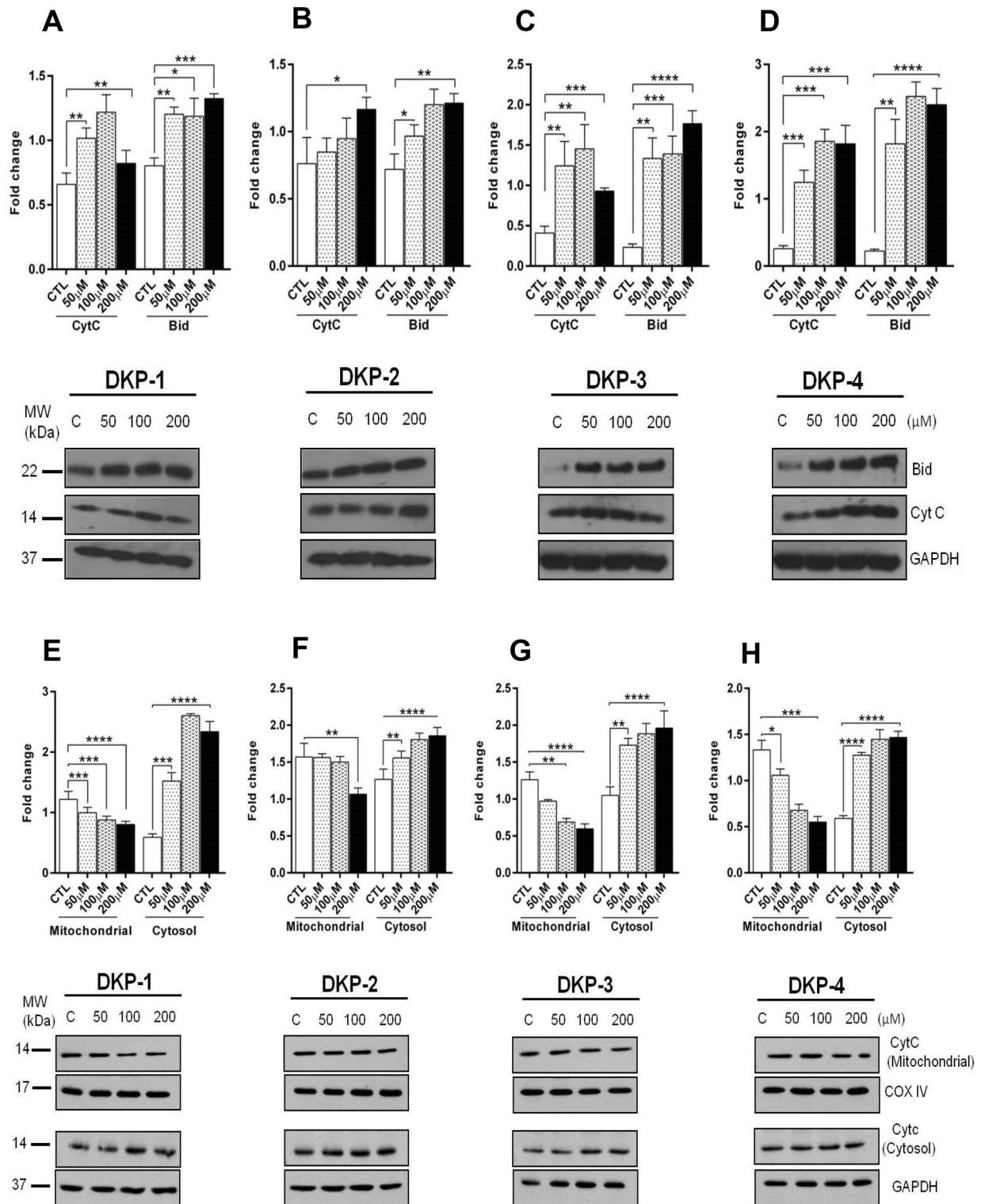


Figure 5. Apoptotic protein expression levels in DKPs treated and un-treated HT-29 cells for 24 h. (A–D) Effect of DKPs on the expression of apoptosis-related proteins in the whole-cell lysate of DKP-1: cyclo (L-Pro-L-Leu) (A), DKP-2: cyclo (L-Pro-L-Val) (B), DKP-3: cyclo (L-Pro-L-Phe) (C), and DKP-4: cyclo (L-Pro-L-Tyr) (D) for 24 h. (E–H) Effect of DKPs on the cytochrome-c levels from the mitochondrial and cytosolic fraction of DKP-1: cyclo (L-Pro-L-Leu) (E), DKP-2: cyclo (L-Pro-L-Val) (F), DKP-3: cyclo (L-Pro-L-Phe) (G), and DKP-4: cyclo (L-Pro-L-Tyr) (H). Western blot analysis was performed using antibodies against CytC, Bid, and GAPDH served as a housing gene. Data were presented as the mean \pm SD (n = 3). Data were analyzed by one-way ANOVA with student’s two-tailed *t*-test. The asterisks **p* < 0.05, ***p* < 0.001, ****p* < 0.0001, *****p* < 0.0001, indicates a significant difference between the control in response to DKPs treatments. The groupings were cropped from different gels subjected to identical conditions. Full blots were shown in the Supplementary Information, Fig. S4A–H.

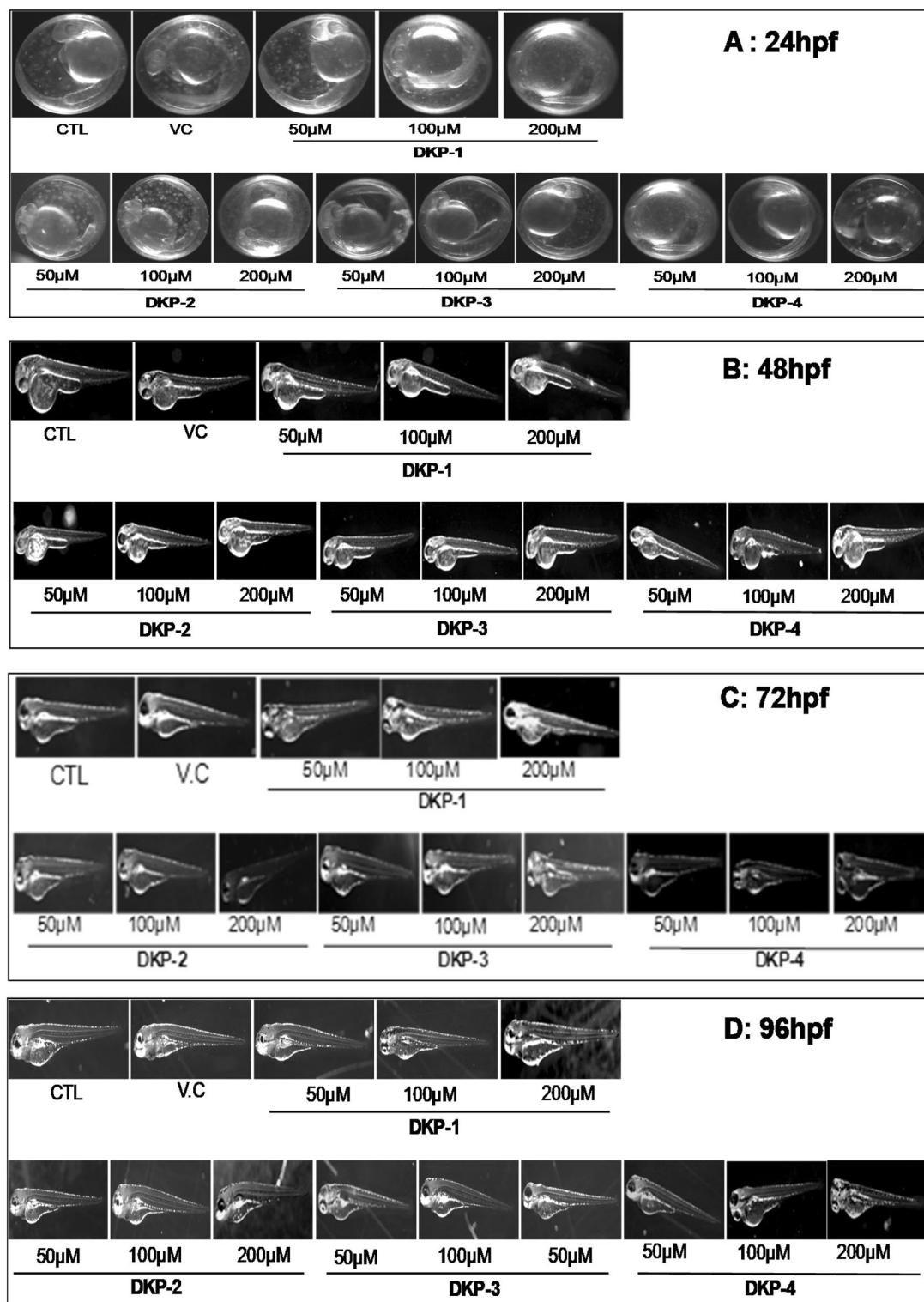


Figure 6. Developmental changes in the zebrafish embryos after treatment with different doses of four cyclic dipeptides. Representative images for 24 hpf (A), 48 hpf (B), 72 hpf (C), and 96 hpf (D). CTL Control, DMSO Vehicle control (DMSO).

colon cancer cells with IC_{50} values of 0.53 and 0.66 mg/mL, respectively¹³. A new cyclic dipeptide petrocidin-A was isolated from *Streptomyces* sp. SBT348, which exhibited significant anti-proliferative effects towards HL-60 and HT-29 cells with IC_{50} values of 3.9 and 5.3 μ g/mL^{28,29}. Moreover, cyclo (L-Leu-L-Pro) exhibited anticancer effects against three leukemic cell lines at a concentration of less than 100 μ g/mL³⁰. A possible explanation

for the low and high peptide concentrations required for significant growth inhibition of various cancer cells described above is owing to several factors including the possibility of DKPs binding to serum proteins in the culture medium, and drug efflux by P-glycoprotein, or the lack of sufficient absorption of peptides into the cells²⁵.

A key mechanism involved in the action of many anticancer drugs is the activation of extrinsic and intrinsic apoptotic pathways^{31–34}. The crucial element in the intrinsic apoptotic pathway is the efflux of Cytc from mitochondria to the cytosol. In the cytosol, Cytc together with apoptotic protease activating factor 1 (Apaf-1) activates Casp-9, which activates Casp-3 as a key execution of apoptosis. In both pathways, the initiator caspase cleaves and activates downstream effector caspase, such as Casp-3³⁵. In this study, we noted that all DKPs induce early and late apoptotic cell death of HT-29 cells in a dose-dependent manner. Taken together, both MTT and apoptosis analysis revealed that four DKPs are robustly inhibiting the proliferation of colon adenocarcinoma cells by the induction of apoptosis. Further, we observed the expression levels of apoptotic (Cytc, Casp-3 and Bid) and anti-apoptotic (Bcl-2) markers were up- and down-regulated in HT-29 cells in response to DKPs treatments. A possible explanation for the significant up-regulation of Casp-3 in DKPs treated cells, in this study may be activated by an initiator caspase such as Casp-9^{36,37}. However, all DKPs induces apoptosis by directly activating Casp-3 or by cleaving Bid (BH3 interacting-domain death agonist), resulting in mitochondrial dysfunction and subsequent release of Cytc and activation of Casp-9 and Casp-3¹⁷. Our findings are supported by an earlier study, where the expression of apoptotic genes was significantly up-regulated in oral squamous cancer after treatment with isocudraxanthone K³⁶. Lee and co-workers also reported that anthocyanin, the derivative of the flavonoid family, which induces apoptosis of leukaemia U937 cells by down-regulating Bcl-2 expression³⁷. Our observations are consistent with previous studies suggesting that mitochondria play an important role in cell survival and mitochondrial-mediated apoptosis by modulating the balance of pro and anti-apoptotic Bcl-2 family proteins^{38–40}. Besides, DKPs were isolated from *P. aeruginosa* PAO1, which induces apoptosis in caspase-9-dependent pathway⁴¹. Overall, our findings reveal that DKPs induces apoptosis in HT-29 cells by the activation of a mitochondria-mediated apoptotic pathway.

In recent years, zebrafish become a suitable model for oncology research using the approach of xenotransplantation of human cancer cells into the yolk sac of a zebrafish embryo. Nowadays, zebrafish embryos are widely used to study the toxicity assessment of various drugs and bioactive metabolites due to its experimental reliability and also low expansive model^{42,43}. Our toxicity study revealed that four DKPs did not show any significant mortality rate and developmental changes of the zebrafish embryos after exposure with 96 hpf. Besides, the tested four DKPs had a promising antitumor effect on HT-29 xenograft zebrafish. In agreement with our findings, three anti-angiogenic drugs such as bevacizumab, endostar, and lapatinib were demonstrating a remarkable inhibition of tumor growth in a xenografted zebrafish model within a nonlethal dose range⁴⁴. Fu and co-workers reported that pan-phosphatidylinositol 3-kinase (PI3K) inhibitor LY294002 significantly reduced the xenograft tumor size in zebrafish by decreasing the viability of metastatic cancer cells⁴⁵. Furthermore, small-molecule bromodomain-containing protein-4 (BRD4) inhibitor displayed a potent antitumor effect on the zebrafish breast cancer model by targeting BRD4 without causing any cytotoxic effect⁴⁶. To the best of our knowledge, we report for the first time, DKPs have an antitumor therapeutic potency as a lead drug of CRC in vivo zebrafish xenograft model.

In conclusion, four DKPs were isolated and identified from the ethyl acetate extract in the cell free-filtrate of *E. acetylicum* S01, for the first time in this study. These four DKPs were inhibited cell growth arrest and the induction of apoptosis through the activation of the mitochondria-mediated apoptotic pathway (Fig. S6). Moreover, in vivo results revealed that tested four DKPs significantly inhibited tumour progression in a zebrafish xenograft model. Overall, our findings suggest that cyclic dipeptides would be promising drug candidates for CRC therapeutics. This finding paves the path for future studies into the activation and regulation of the mitochondria-mediated apoptotic pathway in CRC by proline-rich cyclic peptides.

Materials and methods

Bacterial strain, extraction, and purification of bioactive compounds. Strain *E. acetylicum* S01 was genetically confirmed by 16S ribosomal RNA gene sequencing, and it showed desirable functional probiotic attributes and provided disease resistance against *Aeromonas hydrophila* infection in goldfish (*Carassius auratus*) as described earlier^{47,48}. For identification and characterization of bioactive compound(s), a loopful culture of *E. acetylicum* S01 was grown in Luria–Bertani broth (LB) (casein enzymatic hydrolysate 10 g/L, yeast extract 5 g/L, sodium chloride 10 g/L, pH 7.5 ± 0.2, water 1,000 mL) and incubated on a rotary shaker (120 rpm) at 37 °C. When the absorbance of the culture was approximately 1.5 at 600 nm, the log phase culture was transferred aseptically into the 400 mL sterile medium and incubated in an orbital shaker at 37 °C for 72 h. The fermented cultures were then centrifuged (6,500 × g, 15 min at –4 °C) followed by filtration through a 0.45-µm filter, to obtain the cell-free culture filtrate. The cell-free supernatants (25-L) obtained after cultivation of the strain S01 in a 1-L conical flask for 96 h were then extracted twice with an equal volume (1:1 ratio) of ethyl acetate and the organic layer was concentrated by rotary evaporator (IKA-RV10, Switzerland). After concentration, the crude extract was yielded 1.3 g/25 L of culture filtrate.

Purification and structure elucidation of bioactive compounds. The oily reddish-yellow residue S01 (1.3 g) obtained after drying was then loaded on a silica gel column (30 cm × 2 cm) previously equilibrated with hexane and eluted consecutively using a linear gradient hexane/ethyl acetate (80:20, 70:30, 60:40, 50:50, 40:60, 30:70, v/v) followed by chloroform/methanol (9:3, v/v) was finally added into the column for elution. The ethyl acetate extract yielded four compounds of pale yellow crystalline nature. The structural elucidation of the isolated compounds was determined by nuclear magnetic resonance (NMR) spectroscopy (Bruker DRX-500-MHz, Rheinstetten, Germany) using denuded chloroform (CDCl₃) as a solvent. ¹H and ¹³C NMR spectra were recorded at ambient temperature at 500-MHz equipped with a 2.5-mm microprobe. Chemical shifts were

Concentration in μM	DKP-1	DKP-2	DKP-3	DKP-4
24 hpf				
CTL	73.33 \pm 0	73.33 \pm 0	73.33 \pm 0	73.33 \pm 0
50	70.88 \pm 3.44	77.77 \pm 5.41	80 \pm 5.96	79 \pm 3.96
100	73.33 \pm 5.96	82.22 \pm 4.41	80 \pm 5.96	82 \pm 2.96
200	75 \pm 5.77	75.55 \pm 3.44	75.55 \pm 4.12	71.55 \pm 5.12
48 hpf				
CTL	71.11 \pm 3.44	71.11 \pm 3.44	71.11 \pm 3.44	68.88 \pm 2.66
50	70.88 \pm 5.96	80 \pm 5.96	80 \pm 5.96	79 \pm 3.96
100	71.11 \pm 1.54	80 \pm 5.96	80 \pm 5.96	81 \pm 2.96
200	73.33 \pm 3.32	75.55 \pm 3.44	75.55 \pm 4.12	70.34 \pm 3.33
72 hpf				
CTL	68.88 \pm 3.44	68.88 \pm 3.44	68.88 \pm 3.44	68.88 \pm 3.44
50	71.11 \pm 3.44	68.88 \pm 3.44	77.77 \pm 9.10	75.51 \pm 3.32
100	71.11 \pm 5.55	77.33 \pm 3.44	80 \pm 5.96	79.3 \pm 2.77
200	68.88 \pm 6.91	71.11 \pm 6.88	73.33 \pm 5.96	70.54 \pm 3.51
96 hpf				
CTL	68.88 \pm 3.44	66.66 \pm 3.44	68.88 \pm 3.44	68.88 \pm 3.44
50	66.66 \pm 5.96	66.66 \pm 5.96	68.88 \pm 6.88	71.11 \pm 2.44
100	71.11 \pm 9.10	71.11 \pm 9.10	80 \pm 5.96	79.3 \pm 2.77
200	66.66 \pm 5.96	66.66 \pm 5.96	69.22 \pm 12	68.24 \pm 5.89

Table 3. Mean survival rates (in three replicates) of DKPs treated and untreated zebrafish embryos. Data are represented as mean \pm SD ($n=3$). DKP-1: cyclo (L-Pro-L-Leu) (A), DKP-2: cyclo (L-Pro-L-Val) (B), DKP-3: cyclo (L-Pro-L-Phe) (C), and DKP-4: cyclo (L-Pro-L-Tyr) (D). hpf – hours post fertilization; CTL Control.

referred to as CDCl_3 (δH 7.26 and δC 77.0), which is given in parts per million (ppm) and coupling constant in Hertz. The compounds were analyzed by a high-resolution mass spectrophotometer (HRMS) and m/z values were obtained using the electrospray ionization mode (Orbitrap LC-Mas, Thermo Scientific Exactive, Waltham, USA) equipped with a BEH C-18 column (2.1×50 mm, Waters, Milford, USA). The specific optical rotation of the compounds was measured using a Jasco P-2000 digital polarimeter coupled with a sodium lamp (Na) at a wavelength of $\lambda 589$ nm. Specific optical rotation was determined by using the following formula:

$$[\alpha]_D^t = \frac{\alpha}{cl}$$

where α = observed rotation, c = concentration (g/mL), l = length of cell (dm), D = yellow of light from sodium lamp, and t = temperature (Celsius).

Cell culture. Human colorectal cancer (HT-29) and mouse embryonic fibroblast (3T3) cells were obtained from the American Type Culture Collection Centre (ATCC, VA, USA). Both cells were grown in Dulbecco Modified Eagle's Medium (DMEM, HiMedia, India) supplemented with 10% heat-inactivated fetal bovine serum (FBS), penicillin (50 units/mL), and streptomycin (50 $\mu\text{g}/\text{mL}$) and were cultured at 37 $^\circ\text{C}$, 5% CO_2 in a humidified atmosphere.

Cell viability by the MTT assay. Cytotoxicity of the identified those DKPs were determined by cell viability study with the MTT (3-(4, 5-dimethylthiazol-2-yl)-2, 5-diphenyltetrazolium bromide) reduction assay⁴⁹. Briefly, 1.5×10^4 cells/well (HT-29) and 1.7×10^4 cells/well (3T3) cells were seeded into 96-well plates. They were incubated for 24 h at 37 $^\circ\text{C}$ with 5% CO_2 and 95% relative humidity atmosphere. After 24 h, identified DKPs were added different concentrations (12.5 to 200 μM) into culture media in triplicates and re-incubated under the same culture conditions mentioned above. The final concentration of DMSO solution was 0.25% in the cells served as a negative control. Then culture media was removed from the plates, and 100 μL of freshly prepared MTT solution in serum-free medium (5 mg/mL) was added to each well and further incubated for 4 h. After that, 150 μL of DMSO solution was added under dark conditions and kept for 30 min at room temperature. The absorbance of the formazan product was measured at 595 nm in the microplate reader (Imark, Biorad). The percentage viability of the cells was measured by using the formula: Cell viability (%) = [(test/control) \times 100].

Apoptosis analysis by Annexin-V/PI staining. The dead, necrotic, and apoptotic cells were analyzed by annexin V/PI double staining method, which was used to detect the externalization of phosphatidylserine (PS). Briefly, cells at the density of 4.5×10^4 cells/well were seeded into 6-well plates and treated with or without DKPs for 24 h. Subsequently, both floating and adherent cells were harvested by centrifugation at 1,500 rpm for 5 min, then re-suspended in 300 μL of 1X binding buffer, followed by 3 μL of annexin V-FITC and propidium

Figure 7. Antitumor effects of four cyclic dipeptides in a zebrafish xenograft model. On 2 dpf, CM-Dil labelled HT-29 xenografted embryos in DKPs treated and un-treated larvae for 72 h. Representative fluorescent images showing DKPs treated and un-treated HT-29 xenograft zebrafish larvae at 0 hpi, 24 hpi, 48 hpi and 72 hpi respectively (A). Quantification of the fluorescence intensity of tumor (B). Tumor growth inhibition rates were calculated according to the fluorescence intensities of the tumor (C). Bar graph showing the survival rate of DKPs treated and un-treated xenografted zebrafish larvae (D). Data were analyzed by one-way ANOVA with student's two-tailed *t*-test. The asterisks **p* < 0.05, ***p* < 0.001, ****p* < 0.0001, *****p* < 0.0001, indicates a significant difference between the control in response to DKPs treatments. CTL Control; Scale bar = 200 μm. The groupings were cropped from different zebrafish/tumor xenograft images subjected to identical conditions. Full zebrafish xenograft embryos were shown in the Supplementary Information, Fig. S5A-D. CTL Control.

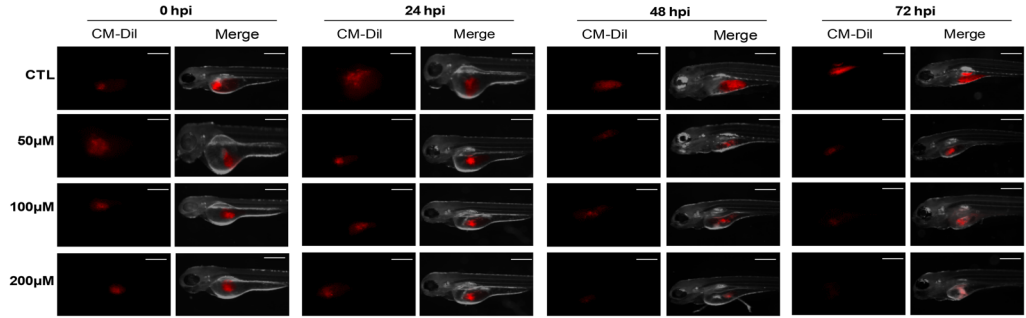
iodide (PI) (Apoptosis Detection kit, Lead Gen, Taiwan) was added into each sample and incubated for 20 min at room temperature in the dark following the protocol recommended by the manufactures. Cells were analyzed by flow cytometry (FACS Calibur, Becton Dickinson, CA, USA) using WinMDI 2.9 software (La Jolla, CA, USA). The individual populations can be defined using quadrant gates, the number of cells in each quadrant indicated the following: Quadrant-1 (Q1): annexin V/PI⁺ cells were considered as dead cells; Quadrant-2 (Q2): Annexin V⁺/PI⁺ cells were considered as late apoptotic and necrotic cells; Quadrant-3 (Q3): Annexin V⁺/PI⁻ cells were considered as early apoptotic cells; Quadrant-4 (Q4): Annexin V/PI⁻ cells were considered as healthy. Data were analyzed using FlowJo V12.1 software (Tree stat, Stanford, CA, USA).

RNA isolation and gene expression analysis. Total RNA was isolated from HT-29 cells using the TRIzol reagent (TaKara, Japan) following the manufacturer's instruction. The quantity and quality of each RNA sample were analyzed with a NanoDrop-1000 (Thermo Fisher Scientific, USA), followed by conversion to cDNA using RevertAid cDNA synthesis kit (Thermo Fisher Scientific, CA, USA) using 1 μg of mRNA to synthesize cDNA. Semi-quantitative reverse transcriptase-polymerase chain (sqRT-PCR) reaction was carried out in a Veriti Thermal Cycler (Applied Biosystems, CA, USA) using 2X Taq DNA polymerase Master Mix RED (Ampliqon, Denmark, Germany) as we previously described method⁴⁸. Primer sequences for sq-RT-PCR are listed in Table 4. All sqRT-PCRs were run for at least three times. GAPDH served as a housekeeping gene to normalize the expression levels. The expression levels were analyzed by measuring the intensity of the band from the gel using Image-J software.

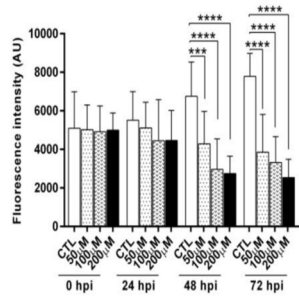
Western blot analysis. Total protein was isolated from HT-29 cells by using lysis buffer. Cells were collected by centrifugation at 1,500 rpm for 5 min. After that, cell pellets were re-suspended with RIPA lysis buffer consisting of 1 mM protease inhibitor cocktail (PIC; Sigma-Aldrich; P8340) and lysed at -4 °C for 1 h. After incubation, the protein was obtained by centrifugation at 13,000 × *g* for 15 min and kept for -80 °C until analysis. Also, mitochondrial and cytosolic fractions were obtained by using fraction lysis buffer as described previously⁵⁰ with minor modifications. Lysed cells were kept in ice for 10 min and then cells were triturated by a 27 gauge syringe (25 strokes) to become homogeneous followed by centrifugation at 13,000 × *g* for 30 min. The collected supernatant was the cytosolic fraction. After the pellet was washed with lysis buffer and it was dissolved in lysis buffer for protein quantification. Protein concentration was measured by Pierce BCA protein assay kit (Thermo Scientific Laboratories, Rockford, USA) according to the manufacturer instructions. Equal amounts of proteins from all samples were separated by 10% SDS-polyacrylamide gel electrophoresis (SDS-PAGE) and electrotransferred. Polyvinylidene difluoride (PVDF) membrane was blocked with 5% skimmed milk for 1 h, followed by incubation with primary (Cytochrome-c: sc-13560; Bid: sc-11423; COX-IV: #4850; 1:2000; GAPDH: #3683; 1:10,000) and HRP-conjugated secondary (Got Anti-mouse IgG: 20102; Got anti-rabbit IgG: 20202: 1:10,000) antibodies against specific proteins. The protein signals were detected by Enhanced Chemiluminescence (ECL) detection kit (Amersham Piscataway, NJ, USA). The protein expression levels were analyzed by measuring the intensity of the band from scanned films using Image-J software. GAPDH and COX-IV served as a housekeeping protein to normalize the expression levels.

Zebrafish husbandry and toxicity assay. Laboratory animal care principles were followed and experimental procedures were conducted following guidelines established by the Institutional Animal Care, and Use Committee (IACUC), and every effort was made to minimize suffering. This study was approved by the IACUC of the Kaohsiung Medical University, Kaohsiung, Taiwan (Approval No: KMU-IACUC-105213). The wild-type (ABiC strain) zebrafish (*Danio rerio*) were maintained at 28 °C on a 14 h/10 h light/dark cycle under standard circulating water systems and fed with hatched brine shrimp. Embryos were obtained by natural mating male fish with female fish (2:3) in a water tank and eggs were maintained in a plastic Petri dish containing ad libitum water. After 4 h incubation, embryos were randomly divided into five experimental groups (control (without treatment), sham/vehicle control (DMSO), and three treatment groups for each cyclic dipeptide. Each group had 45 embryos per test dosage. All DKPs were tested at different doses varied from 50, 100 and 200 μM, respectively. After drug treatment, embryos were maintained in an incubator at 28 °C. The survival rate and embryonic devel-

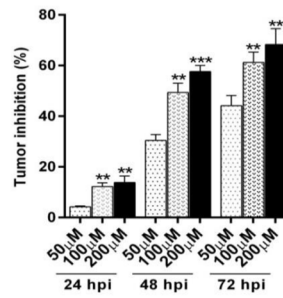
A: Antitumor activity of DKP-1



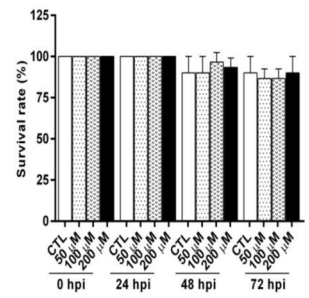
B: Tumor fluorescence intensities



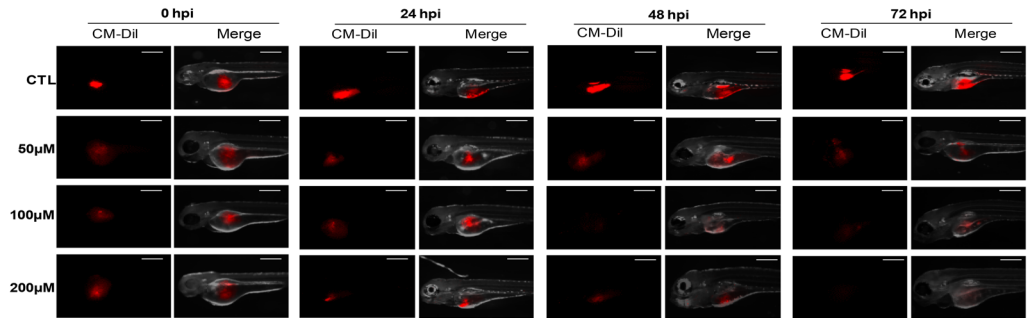
C: Inhibition in tumor



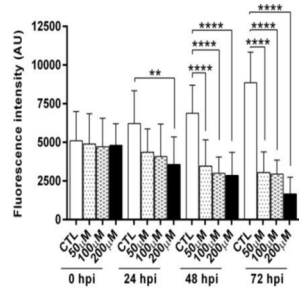
D: Survival rate



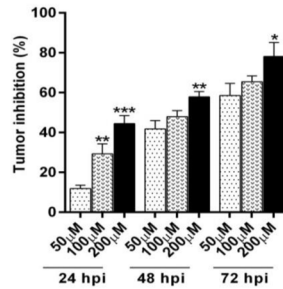
A: Antitumor activity of DKP-2



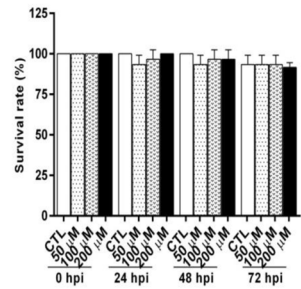
B: Tumor fluorescence intensities



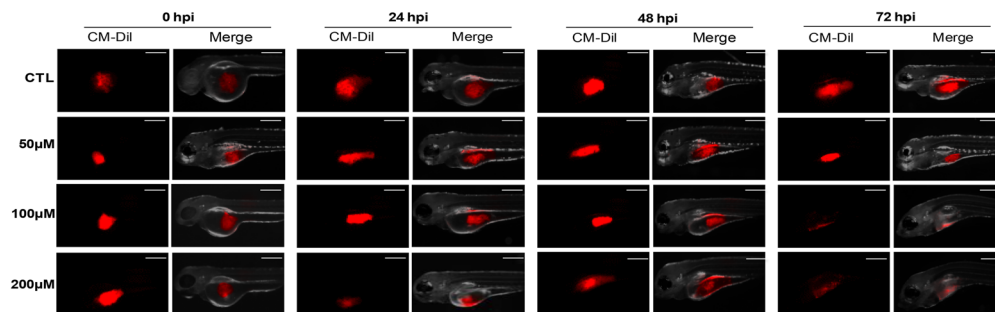
C: Inhibition in tumor



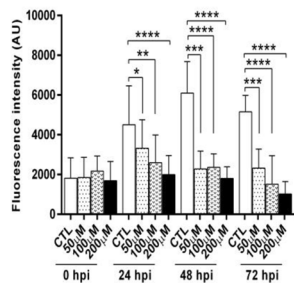
D: Survival rate



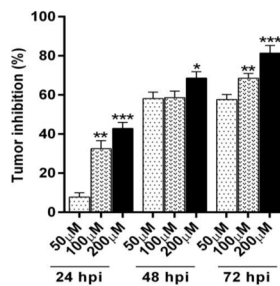
A: Antitumor activity of DKP-3



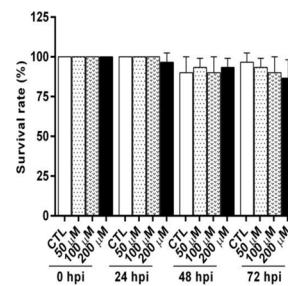
B: Tumor fluorescence intensities



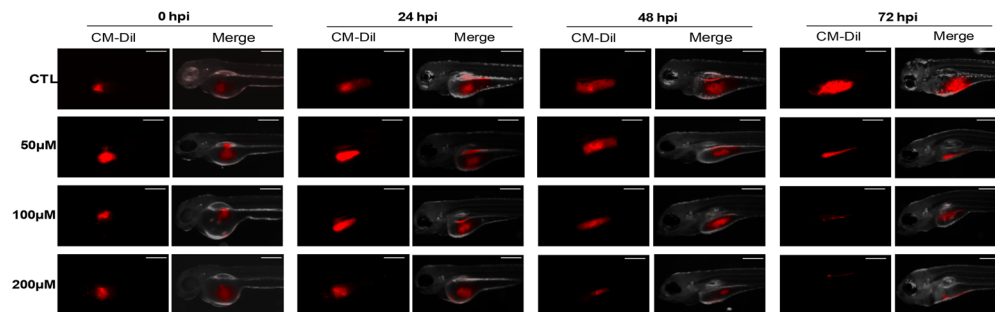
C: Inhibition in tumor



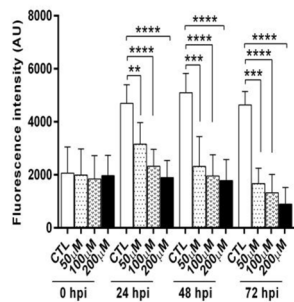
D: Survival rate



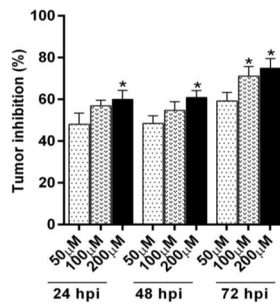
A: Antitumor activity of DKP-4



B: Tumor fluorescence intensities



C: Inhibition in tumor



D: Survival rate

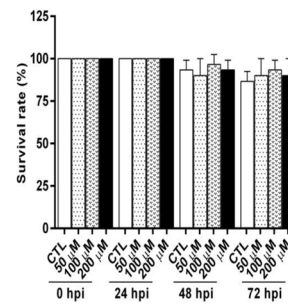


Figure 7. (continued)

Gene	Amplicon size	Anneal	Primer (5'-3')
Bcl-2	267 bp	55 °C—35 s	FWD: CTTTGAGTTCGGTGGGGTCA
			REV: TGGTGATGTGAGTCTGGGCT
Casp-3	275 bp	59 °C—40 s	FWD: GCAGCAAACCTCAGGAAAC
			REV: TGTCCGCATACTGTTTCAGCA
Cytc	302 bp	55 °C—40 s	FWD: AAAAGAGGTGAGAGCGGGTC
			REV: TGGTTGCTGAAGGGCTATGG
GAPDH	576 bp	59 °C—40 s	FWD: CCATCACCATCTCCAGGAG
			REV: CCTGCTTACCACCTTCTTG

Table 4. List of primers used for sqRT-PCR amplifications. *Bcl-2* B-cell lymphoma 2, *Casp-3* Caspase-3, *Cytc* Cytochrome-c, *GAPDH* Glyceraldehyde 3-phosphate dehydrogenase.

opmental changes were observed by using an inverted microscope every 24 h interval for 96 h (Nikon Eclipse TE2000-U, Tokyo, Jap).

Zebrafish and tumor xenograft model. For cell labelling, HT-29 cells were incubated with cell tracker CM-Dil (Invitrogen, Carlsbad, CA, USA) dye at a final volume was 20 μ L/mL for 25 min at 37 °C. To remove the unstrained dye, cells were washed twice and re-suspended with 1X PBS, pH 7.4 to a final density of 2.1×10^6 cells/mL. Prior transplantation, CM-Dil labelled cells were assessed for viability using trypan blue exclusion assay. More than >90% of viable cells were used. For xenotransplantation, 48-hours post-fertilization (hpf) wild-type ABiC embryos were anaesthetized in 0.01% tricaine methanesulfonate (Sigma-Aldrich; MS222) solution containing 0.3% phenylthiocarbamide (PTU; Sigma-Aldrich; P7629). After anesthetization, CM-Dil (a lipophilic fluorescent tracking dye) labelled HT-29 cells grafted into the yolk sac of each zebrafish embryos by using a microinjector IM-300 (Narishige, Tokyo, Japan). After injection, embryos were incubated for 1 h at 28 °C. For confirmation of the visible cell mass at the injection site, zebrafish were transferred to an incubator and maintained at 37 °C.

Xenograft model for antitumor assay. Five hundred CM-Dil labelled HT-29 xenograft zebrafish embryos were randomly selected and hosed into 4 replicate wells in 12-well cell culture plates (5 embryos/well; 20 embryos/treatment group; $20 \times 4 = 80$). The different doses (50, 100 and 200 μ M) of all DKPs were treated with transplanted embryos. Before DKPs treatment, the initial fluorescence intensity of transplanted cancer cells was measured at 0 hour post-injection (hpi). At the end of experiment 24, 48, and 72 hpi, all embryos were selected from each well and were photographed under an inverted fluorescence microscope (Nikon Eclipse TE2000-U, Tokyo, Japan). The following acquisition parameters were employed over time: Image scaling: Low = 130; High = 2,900; Exposure Time = 100 ms and Binning = 1. The fluorescence intensity of the tumor in the embryos was measured and the percentage of tumor growth inhibition was calculated according to the following formula:

$$\text{Inhibition rate(\%)} = \frac{Z(\text{Negative control}) - Z(\text{Treatment})}{Z(\text{Negative control})} \times 100\%$$

Statistical analysis. Results were expressed as mean \pm standard deviation (SD). Data were analyzed one-way analysis of variance (ANOVA), followed by Student's two-tailed *t*-test for comparison between two groups and Dunnett's *t*-test was used when the data involved three or more groups. A value of $p < 0.05$ was considered statistically significant. All statistical analyses and inhibitory concentration (IC_{50}) were determined by graph-prism statistical software (San Diego, CA, USA).

Received: 27 September 2019; Accepted: 30 July 2020

Published online: 13 August 2020

References

- Jemal, A. *et al.* Global cancer statistics. *CA. Cancer J. Clin.* **61**, 69–90 (2011).
- Marmol, I., Sanchez-de-Diego, C., Dieste, A. P., Cerrada, E. & Yoldi, M. J. R. Colorectal carcinoma a general overview and future perspectives in colorectal cancer. *Int. J. Mol. Sci.* **18**, 197 (2017).
- Kukitsu, T. *et al.* Aberrant crypt foci as precursors of the dysplasia-carcinoma sequence in patients with ulcerative colitis. *Clin. Cancer Res.* **14**, 48–54 (2008).
- Yang, S. Y., Sales, K. M., Fuller, B., Seifalian, A. M. & Winslet, M. C. Apoptosis and colorectal cancer: implications for therapy. *Trends Mol. Med.* **15**, 255–233 (2009).
- Prasad, C. Bioactive cyclic dipeptides. *Peptides* **16**, 151–164 (1995).

6. Lau, J. L. & Dunn, M. K. Therapeutic peptides: historical perspectives, current development trends, and future directions. *Bioorganic Med. Chem.* **26**, 2700–2707 (2018).
7. Holden, M. T. *et al.* Quorum-sensing cross-talk: isolation and chemical characterization of cyclic dipeptides from *Pseudomonas aeruginosa* and other gram-negative bacteria. *Mol. Microbiol.* **33**, 1254–1266 (1999).
8. Strom, K., Sjogren, J., Broberg, A. & Schnürer, J. *Lactobacillus plantarum* MiLAB 393 produces the antifungal cyclic dipeptides cyclo(L-Phe–L-Pro) and cyclo(L-Phe–trans-4-OH-L-Pro) and phenyllactic acid. *Appl. Environ. Microbiol.* **68**, 4322–4327 (2002).
9. Graz, C. J. M. *et al.* Cyclic dipeptides in the induction of maturation for cancer therapy. *J. Pharm. Pharmacol.* **52**, 75–82 (2000).
10. NishanthKumar, S., Dileep, C., Mohandas, C., Nambisan, B. & Ca, J. Cyclo (D-tyr-D-phe): a new antibacterial, anticancer, and antioxidant cyclic dipeptide from *Bacillus* sp. N strain associated with a rhabditid entomopathogenic nematode. *J. Pept. Sci.* **20**, 173–185 (2014).
11. Kanoh, K. *et al.* Antitumor activity of phenylalhistin *in vitro* and *in vivo*. *Biosci. Biotechnol. Biochem.* **63**, 1130–1133 (1999).
12. Brauns, S. C., Milne, P., Naude, R. & Venter, M. V. D. Selected cyclic dipeptides inhibit cancer cell growth and induce apoptosis in HT-29 colon cancer cells. *Anticancer Res.* **24**, 1713–1720 (2004).
13. Vazquez-Rivera, D. *et al.* Cytotoxicity of cyclodipeptides from *Pseudomonas aeruginosa* PAO1 Leads to apoptosis in human cancer cell lines. *BioMed Res. Int.*, **2015**, 1–9 (2015).
14. Evan, G. I. & Vousden, K. H. Proliferation cell cycle and apoptosis in cancer. *Nature* **441**, 342–348 (2001).
15. Jin, Z. & El-Deiry, W. S. Overview of cell death signalling pathways. *Cancer Biol. Ther.* **4**, 139–163 (2005).
16. Arnould, D. *et al.* Mitochondrial release of apoptosis-inducing factor occurs downstream of cytochrome c release in response to several proapoptotic stimuli. *J. Cell. Biol.* **159**, 923–992 (2002).
17. Cory, S. & Adams, J. M. The Bcl-2 family regulators of the cellular life-or-death switch. *Nat. Rev. Cancer* **2**, 647–656 (2002).
18. White, R., Rose, K. & Zon, L. Zebrafish cancer the state of the art and the path forward. *Nat. Rev. Cancer* **13**, 624–636 (2013).
19. Stern, H. M. & Zon, L. I. Cancer genetics and drug discovery in the zebrafish. *Nat. Rev. Cancer* **3**, 533–539 (2003).
20. Pruvot, B. *et al.* Leukemic cell xenograft in zebrafish embryo for investigating drug efficacy. *Haematol. J.* **96**, 612–616 (2011).
21. Nishanth Kumar, D. R. *et al.* Isolation of proline-based cyclic dipeptides from *Bacillus* sp. N strain associated with rhabditid entomopathogenic nematode and its antimicrobial properties. *World. J. Microbiol. Biotechnol.* **29**, 355–364 (2013).
22. Yan, P. S. *et al.* Cyclo(L-Leucyl-L-Prolyl) produced by *Achromobacter xylosoxidans* inhibits aflatoxin production by *Aspergillus parasiticus*. *Appl. Environ. Microbiol.* **70**, 7466–7473 (2004).
23. Jayatilake, G. S., Thornton, M. P., Leonard, A. C., Grimwade, J. E. & Baker, B. J. Metabolites from an antarctic sponge-associated bacterium, *Pseudomonas aeruginosa*. *J. Nat. Prod.* **59**, 293–296 (1996).
24. Arunrattiyakorn, P., Nitoda, T. & Kanzaki, H. Enzymatic conversion-based method for screening cyclic dipeptide-producing microbes. *Peptides* **27**, 633–639 (2006).
25. Bellamy, W. T. P-glycoproteins and multidrug resistance. *Ann. Rev. Pharmacol. Toxicol.* **36**, 161–183 (1996).
26. Kahouli, I., Tomaro-Duchesneau, C. & Prakash, S. Probiotics in colorectal cancer (CRC) with emphasis on mechanisms of action and current perspectives. *J. Med. Microbiol.* **62**, 1107–1123 (2013).
27. Yan, F. *et al.* Soluble proteins produced by probiotic bacteria regulate intestinal epithelial cell survival and growth. *Gastroenterology* **132**, 562–575 (2007).
28. Cheng, C. *et al.* Isolation of petrocidin A, a new cytotoxic cyclic dipeptide from the marine sponge-derived bacterium *Streptomyces* sp. SBT348. *Mar. Drugs* **15**, 383 (2017).
29. Milne, P. J., Hunt, A. L., Rostoll, K., Van-der, W. J. J. & Graz, C. J. M. The biological activity of selected cyclic dipeptides. *J. Pharm. Pharmacol.* **50**, 1331–1337 (1998).
30. Rhee, K. H. Isolation and characterization of *Streptomyces* sp. KH-614 producing anti-VRE (vancomycin-resistant enterococci) antibiotics. *J. Gen. Appl. Microbiol.* **48**, 321–327 (2002).
31. Ron, D. & Walter, P. Signal integration in the endoplasmic reticulum unfolded protein response. *Nat. Rev. Mol. Cell Biol.* **8**, 519–529 (2007).
32. Chou, C. K. *et al.* Ethyl acetate extract of *Scindapsus cf. hederaceus* exerts the inhibitory bioactivity on human non-small cell lung cancer cells through modulating ER stress. *Int. J. Mol. Sci.* **1832**, 2–23 (2018).
33. Yoon, M. J. *et al.* Stronger proteasomal inhibition and higher CHOP induction are responsible for more effective induction of paraptosis by dimethoxycurcumin than curcumin. *Cell Death Dis.* **5**, 1112 (2014).
34. Ashkenazi, A. & Dixit, V. M. Death receptors: signalling and modulation. *Science* **5381**, 1305–1308 (1998).
35. Li, P. *et al.* Cytochrome c and dATP-dependent formation of Apaf-1/caspase-9 complex initiates an apoptotic protease cascade. *Cell* **91**, 479–489 (1997).
36. Shin, M. R. *et al.* Isocudraxanthone K induces growth inhibition and apoptosis in oral cancer cells via hypoxia-inducible factor-1 α . *BioMed Res. Int.* **2014**, 1–14 (2014).
37. Lee, S. H. *et al.* Induction of apoptosis in human leukaemia U937 cells by anthocyanins through down-regulation of Bcl-2 and activation of caspases. *Int. J. Oncol.* **34**, 1077–1083 (2009).
38. Narayan, S., Chandra, J., Sharma, M., Naithani, R. & Sharma, S. Expression of apoptosis regulators Bcl-2 and Bax in childhood acute lymphoblastic leukemia. *Haematology* **12**, 39–43 (2007).
39. Zecchin, K. G. *et al.* High Bcl-2/Bax ratio in Walker tumor cells protects mitochondria but does not prevent H2O-2 induced apoptosis via calcineurin pathways. *J. Bioenerg. Biomembr.* **39**, 186–194 (2007).
40. Saed, G. M., Jiang, Z., Fletcher, N. M. & Diamond, M. P. Modulation of the BCL-2/BAX ratio by interferon-gamma and hypoxia in human peritoneal and adhesion fibroblasts. *Fertil. Steril.* **90**, 1925–1930 (2008).
41. Hernandez-Padilla, L. *et al.* The antiproliferative effect of cyclodipeptides from *Pseudomonas aeruginosa* PAO1 on HeLa Cells involves inhibition of phosphorylation of Akt and S6k Kinases. *Molecules* **1024**, 2–18 (2017).
42. Evensen, L. *et al.* Zebrafish as a model system for the characterization of nanoparticles against cancer. *Nanoscale* **8**, 862–877 (2015).
43. Cabezas-Sainz, P. *et al.* Improving zebrafish embryo xenotransplantation conditions by increasing incubation temperature and establishing a proliferation index with ZF tool. *BMC Cancer* **18**, 1–12 (2018).
44. Jin, Y. *et al.* Comparison of efficacy and toxicity of bevacizumab, endostar and apatinib in transgenic and human lung cancer xenograft zebrafish mode. *Sci. Rep.* **8**, 15837 (2018).
45. Fu, A., Peh, Y. M., Ngan, W., Wei, N. & Luo, K. Q. Rapid identification of antimicrometastases drugs using integrated model systems with two-dimensional monolayer, three-dimensional spheroids, and zebrafish xenotransplantation tumors. *Biotech. Bioeng.* **115**, 2828–2843 (2018).
46. Ouyang L. *et al.* Discovery of a Small-Molecule Bromodomain-Containing Protein 4 (BRD4) Inhibitor that induces amp-activated protein kinase modulated autophagy-associated cell death in breast cancer. *J. Med. Chem.* **60**, 2–24 (2017).
47. Jinendiran, S., Boopathi, S., Sivakumar, N. & Selvakumar, G. Functional characterization of probiotic potential of novel pigmented bacterial strains for aquaculture applications. *Pro Antimicrobial Prot* **11**, 186–197 (2019).
48. Jinendirana, S., Nathan, A. A., Ramesh, D., Sivakumar, N. & Vaseeharan, B. Modulation of innate immunity, expression of cytokine genes and disease resistance against *Aeromonas hydrophila* infection in goldfish (*Carassius auratus*) by dietary supplementation with *Exiguobacterium acetylicum* S01. *Fish Shellfish Immunol.* **84**, 458–469 (2019).
49. Mosmann, T. Rapid colourimetric assay for cellular growth and survival application to proliferation and cytotoxicity assays. *J. Immunol. Methods* **65**, 55–63 (1983).

50. Kim, H., Moon, J. Y., Ahn, K. S. & Cho, S. K. Quercetin induces mitochondrial-mediated apoptosis and protective autophagy in human glioblastoma U373MG cells. *Oxid. Med. Cell Longev.* **2013**, 1–10 (2013).

Acknowledgements

The authors wish to acknowledge DST– Science Engineering Research Board (SERB), the Government of India for financial support under Young Scientist Scheme (SB/YS/LS–05/2014), and DST-PURSE Phase-II, and UGC-SAP for equipment support. The authors would like to thank Dr. L. Ravi Shankar and Mr. T. Arun Kumar, Chemical Science and Technology Division, CSIR-National Institute for Interdisciplinary Science and Technology, Thiruvananthapuram, India, for permitting to use their laboratory facility for purification and characterization of four cyclic dipeptides. Also, authors wish to thank the Ministry of Science and Technology of Taiwan and Kaohsiung Medical University, for providing a fellowship to Dr. SJ.

Author contributions

S.J. design the experiment, performed the entire experiments, analyzed the data, drafting the manuscript, revising the manuscript and critical review of the final submission. N.S. and B.S.D.K. design the experiment, revising the manuscript and critical review of the final submission. W.T. and W.L. design the zebrafish experiment and verified the results. H.U.D., V.K.P., and C.C.C.C. provided cell culture facility and revising the manuscript. All authors reviewed the manuscript and approved the final submission.

Competing interests

The authors declare no competing interests.

Additional information

Supplementary information is available for this paper at <https://doi.org/10.1038/s41598-020-70516-x>.

Correspondence and requests for materials should be addressed to H.-U.D., B.S.D.K. or N.S.

Reprints and permissions information is available at www.nature.com/reprints.

Publisher's note Springer Nature remains neutral with regard to jurisdictional claims in published maps and institutional affiliations.



Open Access This article is licensed under a Creative Commons Attribution 4.0 International License, which permits use, sharing, adaptation, distribution and reproduction in any medium or format, as long as you give appropriate credit to the original author(s) and the source, provide a link to the Creative Commons license, and indicate if changes were made. The images or other third party material in this article are included in the article's Creative Commons license, unless indicated otherwise in a credit line to the material. If material is not included in the article's Creative Commons license and your intended use is not permitted by statutory regulation or exceeds the permitted use, you will need to obtain permission directly from the copyright holder. To view a copy of this license, visit <http://creativecommons.org/licenses/by/4.0/>.

© The Author(s) 2020